



HAL
open science

Saponite-anthocyanin derivatives: The role of organoclays in pigment photostability

Luciano C.B. Lima, Fabrícia C Silva, Edson C Silva-Filho, Maria G Fonseca,
Guanzheng Zhuang, Maguy Jaber

► To cite this version:

Luciano C.B. Lima, Fabrícia C Silva, Edson C Silva-Filho, Maria G Fonseca, Guanzheng Zhuang, et al.. Saponite-anthocyanin derivatives: The role of organoclays in pigment photostability. Applied Clay Science, 2020, 191, pp.105604. 10.1016/j.clay.2020.105604 . hal-02887368

HAL Id: hal-02887368

<https://hal.sorbonne-universite.fr/hal-02887368v1>

Submitted on 2 Jul 2020

HAL is a multi-disciplinary open access archive for the deposit and dissemination of scientific research documents, whether they are published or not. The documents may come from teaching and research institutions in France or abroad, or from public or private research centers.

L'archive ouverte pluridisciplinaire **HAL**, est destinée au dépôt et à la diffusion de documents scientifiques de niveau recherche, publiés ou non, émanant des établissements d'enseignement et de recherche français ou étrangers, des laboratoires publics ou privés.

1 **Saponite-anthocyanin derivatives: The role of organo-clays in pigment**
2 **photostability**

3

4 *Luciano C. B. Lima^{1,2}, Fabrícia C. Silva^{1,2}, Edson C. Silva-Filho², Maria G. Fonseca³,*
5 *Guanzheng Zhuang^{4,5}, Maguy Jaber^{1*}*

6 ¹Sorbonne Université, CNRS UMR 8220, LAMS, Institut Universitaire de France (IUF), case
7 courrier 225, 4 pl. Jussieu 75252 Paris cedex 05, France

8 ²LIMAV, Univ. Federal do Piauí – UFPI, 64049-550 Piauí, Brazil

9 ³NPE-LACOM, Univ. Federal da Paraíba – UFPB, João Pessoa, 58051-900 Paraíba, Brazil

10 ⁴ CAS Key Laboratory of Mineralogy and Metallogeny, Guangzhou Institute of Geochemistry,
11 Chinese Academy of Sciences, Guangzhou 510640, China.

12 ⁵ Guangdong Provincial Key Laboratory of Mineral Physics and Materials, Guangzhou 510640,
13 China.

14

15 AUTHOR INFORMATION

16 **Corresponding Author**

17 *Tel: +33-(0)1-4427-6289

18 *Email: maguy.jaber@sorbonne-universite.fr

19

20 **ABSTRACT**

21 Hybrid pigments based on organo-saponite (cetyltrimethyl ammonium bromide (CTAB-
22 Sap) and a commercial anthocyanin (ACN) dye, Crystal Red Grape, were prepared. The
23 interactions between organic dye guest and hosts (including saponite and organo-saponite) were
24 investigated by X-ray diffraction, transmission electron microscopy and Fourier transform
25 infrared spectroscopy. The pigments exhibit different colors function of their host-guest
26 interactions. The blue color of organo-clay-anthocyanin indicates the stabilization of quinoidal
27 base form of the dye. The hybrids have good stability against visible light irradiation and basic
28 pH conditions. These dyed materials are environmentally friendly and can be promising
29 candidates in different application fields.

30 Keywords: organo-saponite, anthocyanin, photostability, chemical stability

31

32

33

34

35

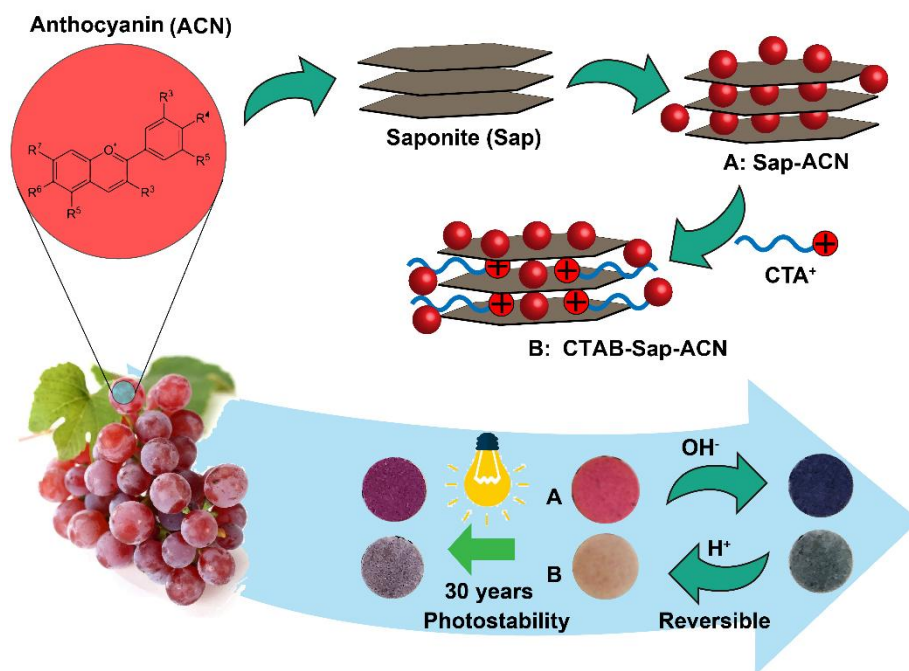
36

37

38

39 GRAPHICAL ABSTRACT

40



41

42 **KEYWORDS:** Saponite, Organo-functionalization, Natural dye, hybrid pigment, Color change.

43

44 **1. Introduction**

45

46 The increasing awareness of consumers regarding food safety has been leading the
47 preference for natural dyes instead of synthetic ones. Anthocyanins (ACN) have an antioxidant
48 and free-radical scavenging properties that make them attractive as substitutes of synthetic dyes.
49 These natural dyes have the 7-hydroxyflavylium cation chromophoric group in their structure
50 which is responsible for most of the purple, blue and red colors of flowers and fruits (Brouillard,
51 1982; Fang et al., 2020). In spite of their potential use in several fields, anthocyanins have
52 limitations due to their photo- and chemical-stabilities (Torres et al., 2011; Silva et al., 2018).
53 Anthocyanin dyes are unstable to external environmental conditions such as light, pH, oxygen,
54 temperature (Piffaut et al., 1994).

55 Therefore, biohybrid compounds that combine these biomolecules and an inorganic
56 substrates such as clay minerals have been widely investigated to reverse these limitations by
57 interaction/protection in the host materials (Kohno et al., 2009; Teixeira-Neto et al., 2012;
58 Pimchan et al., 2014; Lu et al., 2019; Samuei et al., 2020).

59 This strategy is inspired by Maya Blue pigments, in which a variety of clay minerals and
60 organic dyes have been used to prepare stable pigments (Trigueiro et al., 2018; Chen et al., 2019;
61 Zhuang et al., 2019a; Silva et al., 2020). Concerning the ACN stabilization, montmorillonite,
62 synthetic non-swelling mica and silica were employed by Kohno et al., 2009 to improve the
63 stability of ACN against alkaline environment and visible light irradiation. In their study, the best
64 results were obtained by ACN intercalation into montmorillonite. Electrostatic interactions
65 between the intercalated dye and the montmorillonite surface were highlighted and the
66 intercalation protected the dye from atmospheric oxygen (Kohno et al., 2009). Li et al., 2019
67 have reported the acid/base reversible allochroic hybrid pigments prepared by incorporation of

68 ACN on sepiolite, halloysite, kaolinite and montmorillonite. Their comparative study has
69 demonstrated the influence of the clay compositions on color properties, the nanochannels of Sep
70 were claimed to be responsible for the optimum vivid color properties, thermal stability, and
71 chemical corrosion resistance (Li et al., 2019b). Palygorskite was also studied to provide
72 enhancement in ACN stability (Li et al., 2019a).

73 Functionalized clays have also attracted broad attention in the field of lake pigments since
74 they provide better chemical and thermal stability. Recent studies have improved the clay
75 properties by pillaring process (Trigueiro et al., 2018), organo-functionalization with
76 aminosilane (De Queiroga et al., 2019) as well as incorporating a variety of surfactants (Wang
77 and Wang, 2008; Baez et al., 2009; Micó-Vicent et al., 2017). In addition, our group recently
78 reported hybrid pigments with excellent stability by incorporation of alizarin with a variety of
79 organo-modified clays with cetyltrimethylammonium bromide (CTAB) (Silva et al., 2020),
80 Rhodamine 640 perchlorate, sulforhodamine B and Kiton red 620 (Tangaraj et al., 2017) dyes.
81 Despite of the wide use of modified clays to enhance the stabilities of organic dyes, no study
82 explored the stability enhancement for anthocyanin after adsorption on modified clay.

83 This work describes the hybrid pigments formation by adsorption of anthocyanin on
84 saponite (Sap) and an organic modified saponite with cetyltrimethylammonium bromide (CTAB-
85 Sap). These pigments were characterized and their photo- and chemical- stabilities were
86 evaluated.

87

88 **2. Materials and methods**

89 **2.1. Materials**

90

91 Anthocyanin (ACN) source was a Crystal Red Grape (90%, wt) donated by San Joaquin
92 Valley Concentrates (Fresno, CA, USA). cetyltrimethylammonium bromide (CTAB) (99%, wt),
93 citric acid (99.5 %, wt), sodium citrate (99 %, wt), sodium hydroxide (98 %, wt), hydrochloric
94 acid, and other applied chemicals were purchased from Aldrich or Sigma-Aldrich, all with an
95 analytical grade and used without any previous purification.

96

97 **2.2. CTAB-Saponite preparation procedure**

98 2 g of cetyltrimethylammonium bromide (CTAB) were dissolved in 10 mL of 1 mol L⁻¹
99 HCl solution and added dropwise at room temperature to the stirred aqueous suspension of Na-
100 Sap (previously prepared by us (Jaber and Miéché-Brendlé, 2005; Tangaraj et al., 2017). After
101 continuous stirring the mixture at 400 rpm for 3 h, the white precipitate was collected by
102 centrifugation, washed with water until no bromide ion could be detected by an aqueous AgNO₃
103 solution, and then dried at 60°C for 24 h.

104

105 **2.3. Hybrid pigments preparation procedure**

106

107 1 g of Na-Sap or CTAB-Sap were dispersed in 100 mL of anthocyanin (ACN sample
108 donated by San Joaquin Valley Concentrates (Fresno, CA, USA)) citric acid buffer solution at
109 pH 3 (the ACN concentration was 100 mg L⁻¹) and was stirred at 400 rpm for 1 h. The samples
110 were then centrifuged and dried at 50°C overnight. The hybrid pigments samples are named
111 Sap/ACN and CTAB-Sap/ACN.

112

113 **2.4. Characterizations**

114

115 X-ray diffraction were recorded using D8 Advance Bruker-AXS Powder X-ray
116 diffractometer with $\text{CuK}\alpha$ radiation ($\lambda = 1.5405 \text{ \AA}$). Infrared analyzes were performed on Agilent
117 Cary 630 FTIR spectrometer using an Agilent diamond Attenuated Total Reflectance (ATR)
118 technique mode. Thermogravimetric analyses were carried out using a TA Instrument SDT Q600
119 analyzer. The heating rate was of 5°C min^{-1} from 25°C to 1000°C , air flow of $10 \text{ mL} \cdot \text{min}^{-1}$, and
120 using alumina pan. TEM study of the samples was performed on a JEOL 2010 microscope, 200
121 kV LaB6 coupled Orius camera, from Gatan Company.

122

123 **2.5. Chemical stability and photostability**

124

125 Exposure of the hybrid pigments to basic and acidic conditions in a desiccator containing
126 aqueous NH_4OH or HCl to saturate the atmosphere with HCl or NH_3 vapors was carried out,
127 sequentially and repeatedly (Ogawa et al., 2017).

128 The pigments were exposure to white light irradiation for 192 h, using a LED lamp set to
129 provide 100 Klux of illumination intensity, in which this time is equivalent to approximately 32
130 years of exposure in ambient light conditions (Zhuang et al., 2019a, 2019b). The pressed
131 pigments (into pellets) were placed in a desiccator filled with air or nitrogen. The absorbance,
132 reflectance and CIE (Commission Internationale de L'Eclairage) parameters were obtained from
133 an Ocean Optics Halogen and Deuterium Light Source HL-2000-FHSA device as incident light
134 beam and ocean optics USB4000 detector for acquisition. Ocean Optics QP400-1-UV-VIS
135 fiberglass was used to link these devices.

136 The diffuse reflectance (R) converted into equivalent absorption coefficient F(R) using
137 Kubelka–Munk equation (Eq. (1)) (Silva et al., 2018).

138

139
$$F(R) = \frac{(1-R)^2}{2R} \quad (1)$$

140

141 The “Commission Internationale of l’Eclairage” CIE 1976 color space system was applied

142 to evaluate the color of the pigments. Measurements were done on pressed pellets samples as

143 function of L^* , a^* and b^* coordinates. The parameter Lightness (L^*) represents the brightness (+)

144 or darkness (–) of the color, i.e., more positive L^* values refer to whiter while more negative L^*

145 values represent darker. While, the values of a^* and b^* indicate the color details: $+a^*$ is the red

146 direction, $-a^*$ the green direction, $+b^*$ the yellow direction, and $-b^*$ the blue direction (Zhuang et

147 al., 2019b). The differences of colors between unexposed and exposed samples were calculated

148 by $\sqrt{((\Delta L^*)^2 + (\Delta a^*)^2 + (\Delta b^*)^2)}$ equation.

149

150 3. Results and Discussion

151

152 The XRD pattern of the sodium saponite (Fig. 1A) showed the (001) reflection at 7.66°

153 (2θ), corresponding to the basal spacing of 1.16 nm. After organic modification with CTAB, the

154 basal spacing increased to 1.62 nm in CTAB-Sap. This phenomenon indicates that CTA^+ cations

155 successfully intercalated into the interlayer space of Sap by cation exchange with Na^+ . The

156 difference between the Sap layer thickness (0.96 nm) and the basal spacing of CTAB-Sap (1.62

157 nm) was 0.66 nm, which is consistent with a monolayer arrangement of the organic molecules

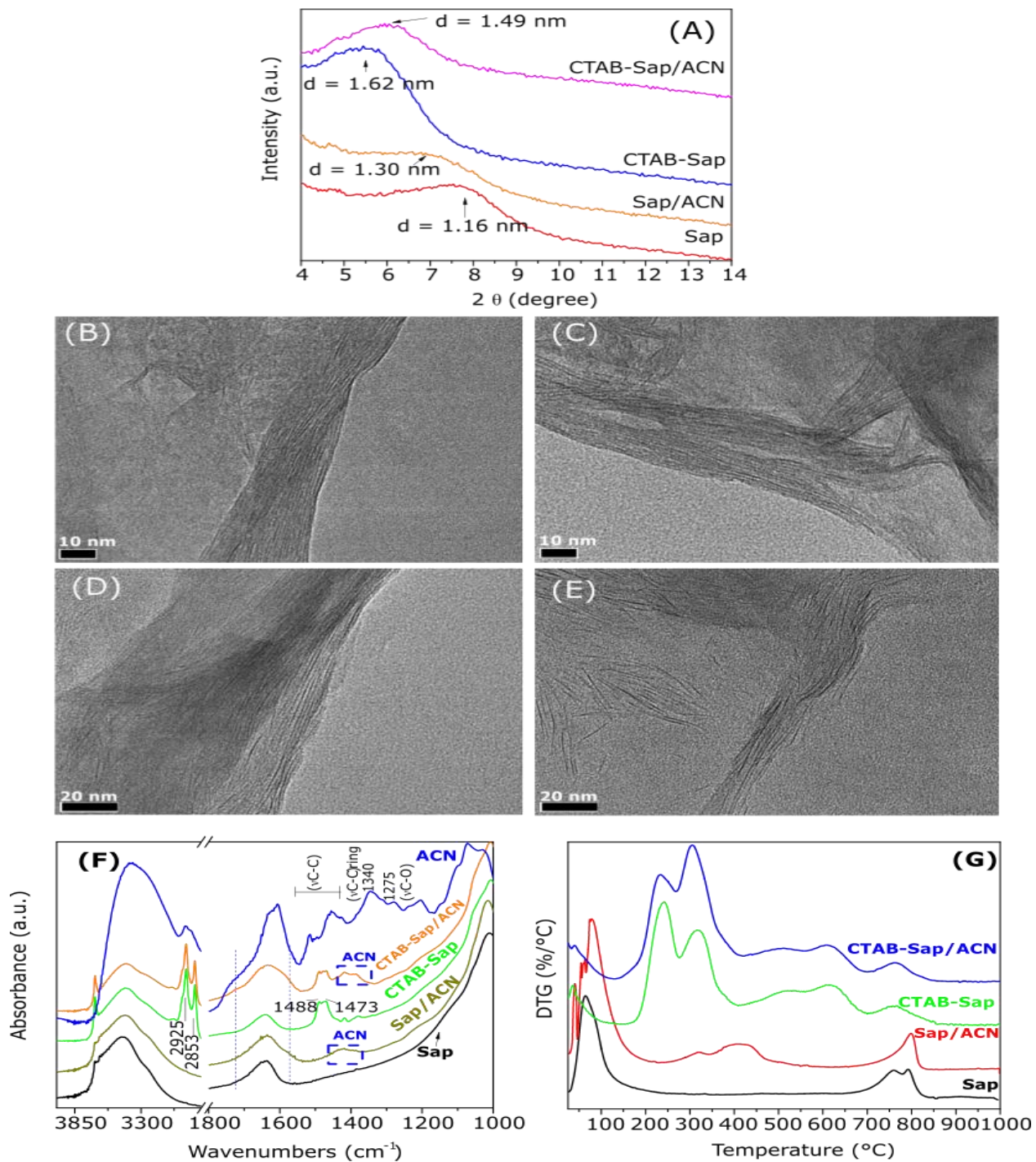
158 considering the dimensions of CTA^+ cations (at about 0.51 nm) (Marçal et al., 2015).

159 After loading with anthocyanin, the (001) reflection of Sap/ACN was broader, however, no

160 significant change was observed in the $d_{(001)}$ values of CTAB-Sap/ACN suggesting a surface (or

161 edge) loading

162 TEM micrographs showed layers with alternate dark and bright fringes allowing the
163 measurement of interplanar distances. For Na-Sap, an interlayer distance of 1.19 ± 0.11 nm was
164 obtained (Figure 1B). In CTAB-Sap, the interlayer distance increased to 1.57 ± 0.19 nm (Figure
165 1C). After loading with anthocyanin molecules, the $d_{(001)}$ spacing were 1.39 ± 0.19 , 1.49 ± 0.20 nm
166 for Sap/An, CTAB-Sap/ACN, respectively (Figure 1 D and E) and some exfoliated layers were
167 observed corroborating with the enlargement of the (001) reflection observed in XRD. .
168



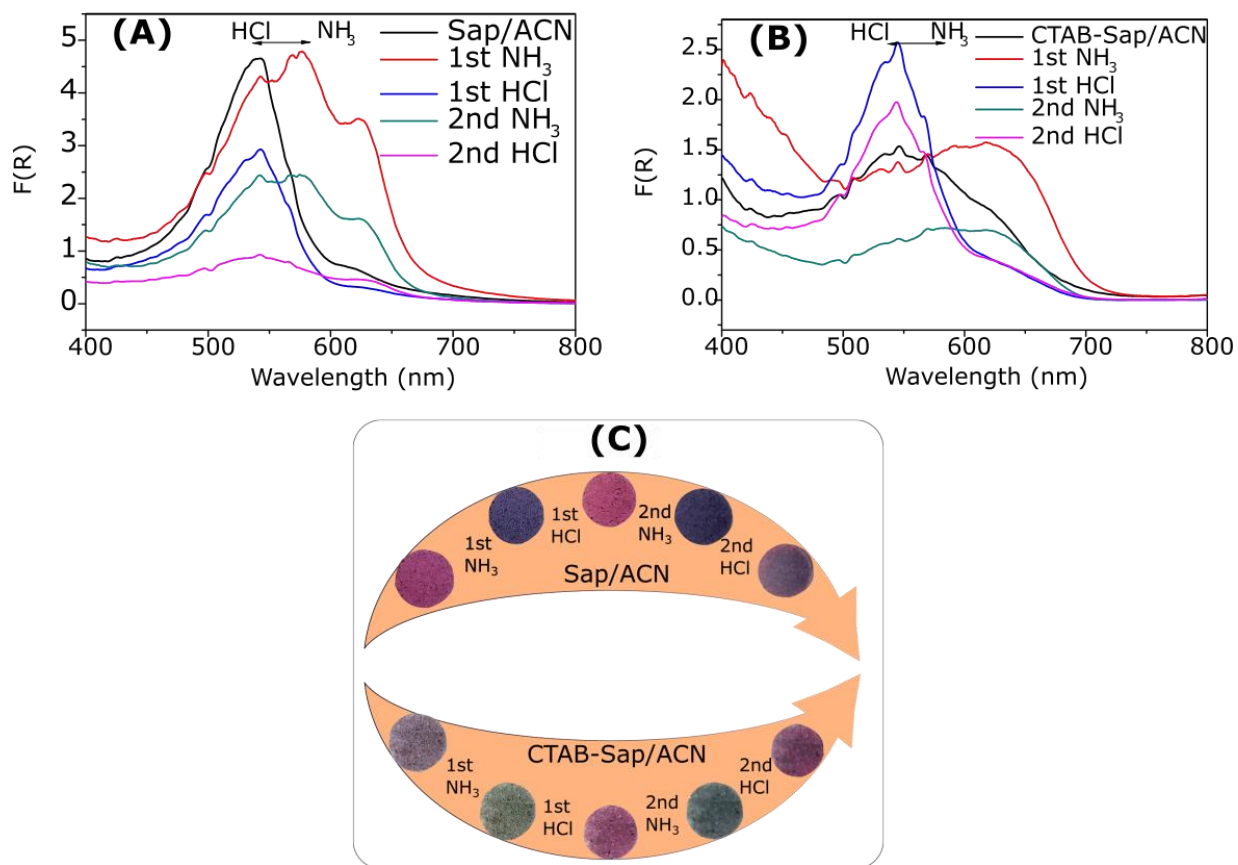
169
 170 **Figure 1.** (A) XRD patterns of Sap, Sap/ACN, CTAB-Sap and CTAB-Sap/ACN; TEM images
 171 of (B) Sap, (C) Sap/ACN, (D) CTAB-Sap and (E) CTAB-Sap/ACN; (F) FTIR spectra of Sap,
 172 Sap/ACN, CTAB-Sap, CTAB-Sap/ACN and (G) DTG curve of Sap, Sap/ACN, CTAB-Sap and
 173 CTAB-Sap/ACN.

174 The FTIR spectra are depicted in Fig.1. For Sap, the sharp and weak band at 3677 cm^{-1} and
175 the one between $3000\text{-}3600\text{ cm}^{-1}$ correspond to the stretching vibration of structural -OH group
176 and adsorbed water, respectively. The band at 1633 cm^{-1} is attributed to the bending vibration of
177 -OH . The band at 980 cm^{-1} was assigned to the Si-O-Si stretching (Tao et al., 2016; Fatimah et
178 al., 2019). Several new bands at 2925 , 2853 , 1488 and 1473 cm^{-1} , which were assigned to the
179 characteristic vibrations of CTAB alkyl chain, emerged in the FTIR spectrum of CTAB-Sap,
180 demonstrating the presence of organic molecules. Concerning the Sap/ACN and CTAB-
181 Sap/ACN samples, the contributions of OH and C=O modes brought from loaded ACN as well
182 as the new hydrogen bond formed in the hybrid pigments make the bands at the regions between
183 $3000\text{-}3760\text{-cm}^{-1}$ and $1550\text{-}1760\text{ cm}^{-1}$ broader than the respective precursor. The signals in the
184 region between $1350\text{-}1470\text{ cm}^{-1}$ are attributed to the contribution of $\nu(\text{C-C})$ in aromatic ring of
185 anthocyanin loaded.

186 In Figure 1G, the first step of mass loss (8%) at $25\text{-}238^\circ\text{C}$ for Na-SAP was assigned to the
187 dehydration of surface and interlayer water. The second event at $640\text{-}859^\circ\text{C}$ is due to
188 dehydroxylation of Sap with a mass loss of 3% (Tangaraj et al., 2017; Zhang et al., 2017). The
189 DTG curve of Sap/ACN shows an additional mass loss of 7% in the region $210\text{-}623^\circ\text{C}$ attributed
190 to the degradation of the incorporated anthocyanin. The mass loss in the second event of CTAB-
191 Sap sample before the ACN adsorption was 30%. After dye loading, the organic mass loss
192 increases to 32% for CTAB-Sap/ACN sample.

193 The hybrid pigments were exposed to HCl or NH_3 saturated atmosphere. The results upon
194 exposure to acidic and basic vapors were monitored by visible absorption spectroscopy and also
195 by visual changes in their photographs, these results are present in Figure 2.

196



197
 198 **Figure 2.** Spectra changes after each step of sequential exposure to acidic and basic atmosphere
 199 for (A) Sap/ACN; (B) CTAB-Sap/ACN. (C) Digital photographs of the color changes of hybrid
 200 pigments upon exposure.

201 Colors changes from red to blue after exposure to basic atmosphere (NH₃ from aqueous
 202 NH₄OH) were observed in the Sap/ACN. The process is reversible, as shown in Figure 2C. The
 203 exposure time to change the color was about 10 min. Similar results were obtained in the
 204 literature.

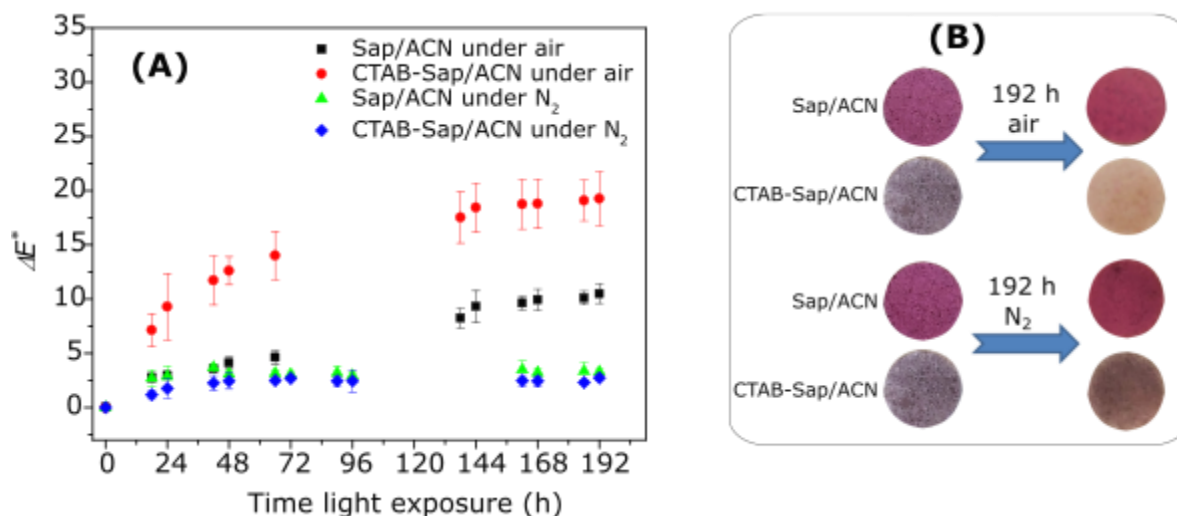
205 In Figure 2A, the absorption band has a redshift after exposure to basic atmosphere, and
 206 return to the same wavenumber, after exposure to basic atmosphere. After several cycles; the
 207 same observations on the spectra were noticed. The color change was reversible and repeatable

208 for at least two cycles. The color changes are still observed after the second cycle of exposure,
209 although strong acid and base conditions degraded the pigments.

210 The contribution of quinoidal base in the anthocyanin molecule in CTAB-Sap/ACN was
211 more pronounced than in the other hybrid and explains its initial blue color. After the first
212 exposure to basic vapor, the right shift observed in Figure 3B is due to the conversion of
213 remaining flavylium cations to quinoidal base, which causes a change only in nuance of blue
214 (Figure 2C). Hybrids being exposed to basic conditions were again submitted to acidic
215 environment, the color of CTAB-Sap/ACN change to red and their spectra were similar to the
216 Sap/ACN, indicating that the anthocyanin molecules became flavylium cation form. The
217 behavior of color change in the following cycles was also similar to the Sap/ACN (Ogawa et al.,
218 2017; Silva et al., 2018; Eskandarabadi et al., 2019; Koosha and Hamed, 2019). The decreases
219 in relative absorbance after the end of four cycles are 80.4% and 73.8% for Sap/ACN, CTAB-
220 Sap/ACN, indicating a slightly better chemical stability for CTAB-Sap/ACN.

221 The colors of solid hybrid pigments were evaluated before and after light exposure during
222 192 h (32 years of exposure in a museum). Measurements of $L^*a^*b^*$ parameters were carried out
223 at different light irradiation time (Figure 3).

224



225
 226 **Figure 3.** (A) Photo-ageing of pigments and (B) digital photographs of color change
 227 observations over 192 h of light exposure in air and nitrogen atmosphere.

228 In solution, the color of ACN changes from red in acid conditions to blue in neutral to
 229 weak alkaline conditions. However, the difference in color presented by the hybrids results from
 230 the different interactions between the host and the guest since the effect of pH on the color was
 231 controlled with the citric acid buffer solution. The color for Sap/ACN is probably due to the
 232 intercalation of ACN molecule in the interlayer space of Sap, which stabilizes the red color of
 233 flavylum cations. While adsorption in the CTAB-Sap/ACN sample probably induced
 234 stabilization of the ACN quinoidal base, leading to a blue color for the hybrid.

235 The ΔE^* value (Figure 3A) is related to total color difference and is indicative of the light
 236 stability of the pigments. Under air, the ΔE^* values of the pigments increased gradually with the
 237 increase of the ageing time. Finally, the values reached 10.5 ± 0.9 for Sap/ACN and 19.3 ± 2.5 for
 238 CTAB-Sap/ACN after 192 h of light exposure. Lower ΔE^* variation in Sap/ACN is probably due
 239 to the protection of the dye in the interlayer space of the saponite, creating an oxygen hindering
 240 and stabilizing the pigments under irradiation. In nitrogen atmosphere, ΔE^* values were lower
 241 after 192 h of light exposure, the ΔE^* values were 2.7 ± 0.2 and 3.3 ± 0.2 for CTAB-Sap/ACN and

242 Sap/ACN, respectively. In addition, when compared the photostability in air with the
243 photostability in nitrogen, the most significant differences were observed for CTAB-Sap/ACN,
244 which corroborate with the greater exposure of ACN molecules to oxygen attack on air
245 atmosphere for these hybrids.

246

247 **4. Conclusion**

248

249 It is known that the quinoidal base form of anthocyanin is less stable than the flavylum
250 one and it occurs in neutral to basic conditions. The stabilization of quinoidal base form was
251 brought by the intermolecular interactions in CTAB-Sap/ACN, since the synthesis of the hybrids
252 were performed at pH 3. In the Sap/ACN pigment, a cation exchange mechanism leads to the
253 intercalation of the flavylum cation of the natural dye. The enhanced stability against visible
254 light irradiation and basic environmental conditions was brought by the intercalation and/or the
255 intermolecular interaction between the dye and the respective host materials. The intercalation of
256 the dye molecules into the interlayer space of saponite in Sap/ACN sample provide more
257 protection against reactive oxygen species. Reversibility in color upon exposure to acidic and
258 basic atmosphere is an evidence for a possible application of the obtained pigments as a sensor to
259 atmospheric acidity, which can be exploited in several cycles if applied in less extreme pH
260 conditions. These dyed materials are environmentally friendly and can be promising candidates
261 in different application fields.

262

263 **Declaration of Competing Interest.**

264 The authors declare that they have no known competing financial interests or personal
265 relationships that could have appeared to influence the work reported in this paper

266

267 **Acknowledgment**

268 We acknowledge the financial support from the CAPES/COFEBUB (Project No. 835/15),
269 CAPES and National Council for Scientific and Technological Development (CNPq, Brazil) for
270 financial support (Grant 310921/2017-1, M.G.F, 307460/2016-9, E.C.S.F.). The authors thank
271 the Île-de-France region and CNRS for funding.

272 **REFERENCES**

- 273 Baez, E., Quazi, N., Ivanov, I., Bhattacharya, S.N., 2009. Stability study of nanopigment
274 dispersions. *Adv. Powder Technol.* 20, 267–272. <https://doi.org/10.1016/j.appt.2009.02.005>
- 275 Brouillard, R., 1982. Chemical Structure of Anthocyanins, in: Markakis, P. (Ed.), *Anthocyanins*
276 *As Food Colors*. Academic Press, pp. 1–40. [https://doi.org/10.1016/b978-0-12-472550-
277 *8.50005-6*](https://doi.org/10.1016/b978-0-12-472550-8.50005-6)
- 278 Chen, H., Zhang, Z., Zhuang, G., Jiang, R., 2019. A new method to prepare ‘Maya red’ pigment
279 from sepiolite and Basic red 46. *Appl. Clay Sci.* 174, 38–46.
280 <https://doi.org/10.1016/j.clay.2019.03.023>
- 281 De Queiroga, L.N.F., França, D.B., Rodrigues, F., Santos, I.M.G., Fonseca, M.G., Jaber, M.,
282 2019. Functionalized bentonites for dye adsorption: Depollution and production of new
283 pigments. *J. Environ. Chem. Eng.* 7, 103333. <https://doi.org/10.1016/j.jece.2019.103333>
- 284 Eskandarabadi, S.M., Mahmoudian, M., Farah, K.R., Abdali, A., Nozad, E., Enayati, M., 2019.
285 Active intelligent packaging film based on ethylene vinyl acetate nanocomposite containing
286 extracted anthocyanin, rosemary extract and ZnO/Fe-MMT nanoparticles. *Food Packag.*
287 *Shelf Life* 22, 100389. <https://doi.org/10.1016/j.fpsl.2019.100389>
- 288 Fang, J.-L., Luo, Y., Yuan, K., Guo, Y., Jin, S.-H., 2020. Preparation and evaluation of an
289 encapsulated anthocyanin complex for enhancing the stability of anthocyanin. *LWT - Food*
290 *Sci. Technol.* 117, 1–8. <https://doi.org/10.1016/J.LWT.2019.108543>

291 Fatimah, I., Rubiyanto, D., Prakoso, N.I., Yahya, A., Sim, Y.-L., 2019. Green conversion of
292 citral and citronellal using tris(bipyridine)ruthenium(II)-supported saponite catalyst under
293 microwave irradiation. *Sustain. Chem. Pharm.* 11, 61–70.
294 <https://doi.org/10.1016/J.SCP.2019.01.001>

295 Jaber, M., Miéhé-Brendlé, J., 2005. Influence du milieu de synthèse sur la cristallisation de
296 saponite: Proposition de mécanisme réactionnel en milieux acide et basique. *Comptes*
297 *Rendus Chim.* 8, 229–234. <https://doi.org/10.1016/j.crci.2004.10.025>

298 Kohno, Y., Kinoshita, R., Ikoma, S., Yoda, K., Shibata, M., Matsushima, R., Tomita, Y., Maeda,
299 Y., Kobayashi, K., 2009. Stabilization of natural anthocyanin by intercalation into
300 montmorillonite. *Appl. Clay Sci.* 42, 519–523. <https://doi.org/10.1016/j.clay.2008.06.012>

301 Koosha, M., Hamed, S., 2019. Intelligent Chitosan/PVA nanocomposite films containing black
302 carrot anthocyanin and bentonite nanoclays with improved mechanical, thermal and
303 antibacterial properties. *Prog. Org. Coatings* 127, 338–347.
304 <https://doi.org/10.1016/J.PORGCOAT.2018.11.028>

305 Li, S., Ding, J., Mu, B., Wang, X., Kang, Y., Wang, A., 2019a. Acid/base reversible allochroic
306 anthocyanin/palygorskite hybrid pigments: Preparation, stability and potential applications.
307 *Dye. Pigment.* 171, 107738. <https://doi.org/10.1016/J.DYEPIG.2019.107738>

308 Li, S., Mu, B., Wang, X., Kang, Y., Wang, A., 2019b. A comparative study on color stability of
309 anthocyanin hybrid pigments derived from 1D and 2D clay minerals. *Materials (Basel)*. 12,
310 1–14. <https://doi.org/10.3390/ma12203287>

311 Lu, Y., Dong, W., Wang, W., Wang, Q., Hui, A., Wang, A., 2019. A comparative study of
312 different natural palygorskite clays for fabricating cost-efficient and eco-friendly iron red
313 composite pigments. *Appl. Clay Sci.* 167, 50–59. <https://doi.org/10.1016/j.clay.2018.10.008>

314 Marçal, L., De Faria, E.H., Nassar, E.J., Trujillano, R., Martín, N., Vicente, M.A., Rives, V., Gil,
315 A., Korili, S.A., Ciuffi, K.J., 2015. Organically Modified Saponites: SAXS Study of
316 Swelling and Application in Caffeine Removal. *ACS Appl. Mater. Interfaces* 7, 10853–
317 10862. <https://doi.org/10.1021/acsami.5b01894>

- 318 Micó-Vicent, B., López-Herraiz, M., Bello, A., Martínez, N., Martínez-Verdú, F.M., 2017.
319 Synthesis of pillared clays from metallic salts as pigments for thermosolar absorptive
320 coatings. *Sol. Energy* 155, 314–322. <https://doi.org/10.1016/j.solener.2017.06.034>
- 321 Ogawa, M., Takee, R., Okabe, Y., Seki, Y., 2017. Bio-geo hybrid pigment; clay-anthocyanin
322 complex which changes color depending on the atmosphere. *Dye. Pigment.* 139, 561–565.
323 <https://doi.org/10.1016/J.DYEPIG.2016.12.054>
- 324 Piffaut, B., Kader, F., Girardin, M., Metche, M., 1994. Comparative degradation pathways of
325 malvidin 3,5-diglucoside after enzymatic and thermal treatments. *Food Chem.* 50, 115–120.
326 [https://doi.org/10.1016/0308-8146\(94\)90106-6](https://doi.org/10.1016/0308-8146(94)90106-6)
- 327 Pimchan, P., Khaorapapong, N., Ogawa, M., 2014. The effect of cetyltrimethylammonium ion
328 and type of smectites on the luminescence efficiency of bis(8-hydroxyquinoline)zinc(II)
329 complex. *Appl. Clay Sci.* 101, 223–228. <https://doi.org/10.1016/J.CLAY.2014.08.004>
- 330 Samuei, S., Rad, F.A., Rezvani, Z., 2020. The influence of intercalated dye molecules shape and
331 features on photostability and thermal stability between LDH layers. *Appl. Clay Sci.* 184,
332 105388. <https://doi.org/10.1016/j.clay.2019.105388>
- 333 Silva, F. de C., Lima, L.C.B., Silva-Filho, E.C., Fonseca, M.G., Jaber, M., 2020. Through
334 alizarin-hectorite pigments: Influence of organofunctionalization on fading. *Colloids*
335 *Surfaces A Physicochem. Eng. Asp.* 587, 124323.
336 <https://doi.org/10.1016/J.COLSURFA.2019.124323>
- 337 Silva, G.T.M., Silva, C.P., Gehlen, M.H., Oake, J., Bohne, C., Quina, F.H., 2018.
338 Organic/inorganic hybrid pigments from flavylum cations and palygorskite. *Appl. Clay*
339 *Sci.* 162, 478–486. <https://doi.org/10.1016/j.clay.2018.07.002>
- 340 Tangaraj, V., Janot, J.-M., Jaber, M., Bechelany, M., Balme, S., 2017. Adsorption and
341 photophysical properties of fluorescent dyes over montmorillonite and saponite modified by
342 surfactant. *Chemosphere* 184, 1355–1361.
343 <https://doi.org/10.1016/J.CHEMOSPHERE.2017.06.126>
- 344 Tao, Q., Fang, Y., Li, T., Zhang, D., Chen, M., Ji, S., He, H., Komarneni, S., Zhang, H., Dong,

345 Y., Noh, Y.D., 2016. Silylation of saponite with 3-aminopropyltriethoxysilane. *Appl. Clay*
346 *Sci.* 132–133, 133–139. <https://doi.org/10.1016/J.CLAY.2016.05.026>

347 Teixeira-Neto, Â.A., Izumi, C.M.S., Temperini, M.L.A., Ferreira, A.M.D.C., Constantino,
348 V.R.L., 2012. Hybrid materials based on smectite clays and nutraceutical anthocyanins from
349 the Açai fruit. *Eur. J. Inorg. Chem.* 5411–5420. <https://doi.org/10.1002/ejic.201200702>

350 Torres, B., Tiwari, B.K., Patras, A., Cullen, P.J., Brunton, N., O'Donnell, C.P., 2011. Stability of
351 anthocyanins and ascorbic acid of high pressure processed blood orange juice during
352 storage. *Innov. Food Sci. Emerg. Technol.* 12, 93–97.
353 <https://doi.org/10.1016/J.IFSET.2011.01.005>

354 Trigueiro, P., Pereira, F.A.R., Guillermin, D., Rigaud, B., Balme, S., Janot, J.M., dos Santos,
355 I.M.G., Fonseca, M.G., Walter, P., Jaber, M., 2018. When anthraquinone dyes meet pillared
356 montmorillonite: Stability or fading upon exposure to light? *Dye. Pigment.* 159, 384–394.
357 <https://doi.org/10.1016/j.dyepig.2018.06.046>

358 Wang, L., Wang, A., 2008. Adsorption properties of Congo Red from aqueous solution onto
359 surfactant-modified montmorillonite. *J. Hazard. Mater.* 160, 173–180.
360 <https://doi.org/10.1016/j.jhazmat.2008.02.104>

361 Zhang, C., He, H., Tao, Q., Ji, S., Li, S., Ma, L., Su, X., Zhu, J., 2017. Metal occupancy and its
362 influence on thermal stability of synthetic saponites. *Appl. Clay Sci.* 135, 282–288.
363 <https://doi.org/10.1016/J.CLAY.2016.10.006>

364 Zhuang, G., Jaber, M., Rodrigues, F., Rigaud, B., Walter, P., Zhang, Z., 2019a. A new durable
365 pigment with hydrophobic surface based on natural nanotubes and indigo: Interactions and
366 stability. *J. Colloid Interface Sci.* 552, 204–217. <https://doi.org/10.1016/J.JCIS.2019.04.072>

367 Zhuang, G., Rodrigues, F., Zhang, Z., Fonseca, M.G., Walter, P., Jaber, M., 2019b. Dressing
368 protective clothing: stabilizing alizarin/halloysite hybrid pigment and beyond. *Dye.*
369 *Pigment.* 166, 32–41. <https://doi.org/10.1016/j.dyepig.2019.03.006>

370